J. Fluid Mech. (2000), *vol.* 418, *pp.* 1–23. Printed in the United Kingdom

High-Reynolds-number gravity currents over a porous boundary: shallow-water solutions and box-model approximations

By MARIUS UNGARISH[1] AND HERBERT E. HUPPERT[2]

[1]Department of Computer Science, Technion, Haifa 32000, Israel

[2]Institute of Theoretical Geophysics, Department of Applied Mathematics and Theoretical Physics, University of Cambridge, Silver Street, Cambridge CB3 9EW, UK

(Received 7 January 1999 and in revised form 7 January 2000)

The behaviour of an inviscid, lock-released gravity current which propagates over a horizontal porous boundary in either a rectangular or an axisymmetric geometry is analysed by both shallow-water theory and 'box-model' approximations. It is shown that the effect of the porous boundary can be incorporated by means of a parameter λ which represents the ratio of the characteristic time of porous drainage, τ, to that of horizontal spread, $x_0/(g'h_0)^{1/2}$, where x_0 and h_0 are the length and height of the fluid initially behind the lock and g' is the reduced gravity. The value of τ is assumed to be known for the fluid–boundary combination under simulation. The interesting cases correspond to small values of λ; otherwise the current has drained before any significant propagation can occur. Typical solutions are presented for various values of the parameters, and differences to the classical current (over a non-porous boundary) are pointed out. The results are consistent with the experiments in a rectangular tank reported by Thomas, Marino & Linden (1998), but a detailed verification, in particular for the axisymmetric geometry case, requires additional experimental data.

1. Introduction

Gravity currents occur whenever fluid of one density flows primarily horizontally into fluid of a different density. Many such situations arise in both industrial and natural settings, as reviewed by Simpson (1997) and Huppert (1998). Commonly the current is driven by compositional or temperature differences, to lead to a homogeneous current, or by suspended particulate matter, to lead to a particle-driven current. Combinations of both particle and compositional or temperature differences can also occur (Sparks *et al.* 1993). Currents may propagate in either a rectangular two-dimensional or cylindrical axisymmetric configuration, or may be otherwise influenced by sidewall and/or topographic constraints. Some of these processes have now been fairly well investigated. The typical problem considers the instantaneous release of a constant volume of heavy fluid from behind a lock into a large reservoir of a lighter fluid above an impermeable horizontal boundary. Our aim here is primarily to evaluate the effects of a porous horizontal boundary on the propagation and shape of high-Reynolds-number homogeneous currents resulting from the instantaneous release of a finite volume in either rectangular two-dimensional or cylindrical axisymmetric geometry. Applications of our work include areas such as oceanography (i.e. currents impinging on coastal shelves) and environmental control (i.e. accidental collapse of storage tanks surrounded by gravel beds).

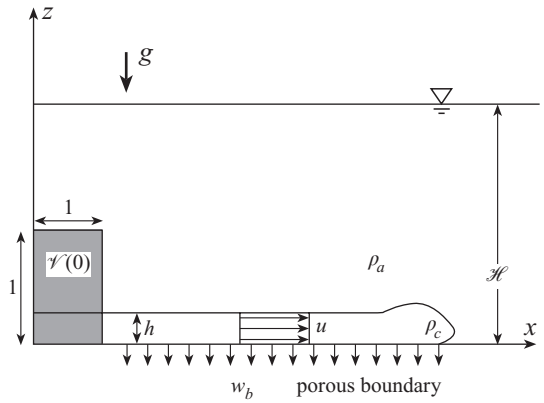

FIGURE 1. Schematic description of the system. In the axisymmetric case z is the axis of symmetry and the horizontal coordinate is the radius, r. The grey region represents the current at $t = 0$. The z-coordinate is scaled with the initial height h_0 of the current, and the horizontal coordinate is scaled with the initial length x_0 (or r_0). The deformation of the upper interface is negligibly small.

Almost the only previous study on this problem has been recently performed by Thomas, Marino & Linden (1998, hereafter referred to as TML). They considered the propagation of a saline current into fresh water in a rectangular container over a porous boundary (which they represented by a thin metallic grid below which a layer of fresh water was placed). They contributed to the understanding of the problem as follows. First, a collection of laboratory experimental data, mainly of distance of propagation as a function of time, was acquired. The maximum propagation distance in the rectangular tank was 195 cm, the additional length of the lock was between 15 and 37 cm, and the height of the ambient fluid, as well as the initial height of the current in the lock, was 20 cm, while the values of g' were 9.8, 49 or 98 cm s^{-2}. Second, an analysis was performed which: suggested a practical correlation for the vertical velocity component on the porous boundary; showed that the volume of the released current decays due to the porous boundary, approximately as $\exp(-t/\tau)$; presented the evaluation of τ for the experimental settings; and showed that viscous forces in the motion of the current above the porous boundary were unimportant (the flow in the porous layer is of course greatly influenced by viscous effects). TML also presented a simple analytical model for correlating the distance of propagation against time t and the parameter τ. However, the integration of these observations into a systematic theory of gravity currents – in particular, the formulation and solution of the shallow-water equations and the development of 'box models' – is still needed, and it is the objective of this paper to supply these results.

The system under consideration is sketched in figure 1: a deep layer of ambient fluid, of density ρ_a, lies above a porous horizontal surface at $z = 0$. Gravity acts in the $-z$-direction. Both rectangular and cylindrical (sector or fully axisymmetric) configurations are of interest. In the rectangular case the system is bounded by parallel vertical smooth impermeable surfaces and the current propagates in the direction labelled x. In the cylindrical case the vertical surfaces are radially directed and form a sector of angle Θ (the full axisymmetric case corresponds to a sector angle of 2π) and the current propagates entirely in the radial direction, r. At time $t = 0$ a given volume of fluid of density $\rho_c > \rho_a$ and kinematic viscosity ν, initially at rest in a box of height h_0 and length x_0 (or a cylinder of height h_0 and radius

r_0), is instantaneously released into the ambient fluid. Either a two-dimensional or an axisymmetric current commences to spread. We assume that the Reynolds number of the horizontal flow, $Re = h_N u_N/\nu$ where the subscript N denotes values associated with the 'nose' of the current, is large and hence viscous effects can be neglected. In the experiments of TML the Reynolds number at the beginning of the motion was typically 5×10^4, and these authors estimated that transition to the viscous regime occurs at $Re = 50$; the inviscid regime was therefore valid for the most significant stage of propagation of the current. While the current propagates, fluid is also absorbed into the porous substrate with an expected double effect: the flow is slowed down due to loss of the effective buoyancy excess, and the practical distance of propagation is limited because the current runs out of fluid.

The corresponding flows over an impermeable surface, in particular in the rectangular configuration, have been extensively studied both experimentally and theoretically. Theoretical investigations successfully using the shallow-water approximation have been conducted. Further simplifications in the form of 'box models' have also been developed for obtaining quick estimates of the global behaviour (see Huppert 1998). An extension of these studies that bears some similarity with the present problem is the situation in which the current consists of a fluid laden with particles (Bonnecaze, Huppert & Lister 1993; Bonnecaze *et al.* 1995; Ungarish & Huppert 1998). During the propagation, the heavier particles settle from the current. This causes the flow to slow down and finally stop after a finite distance of propagation when the current runs out of particles.

Our task here is to incorporate the drainage effect of the porous substrate into the modelling of the flow and to understand its main influence. Loosely speaking, the vertical velocity component on the horizontal boundary, with an appropriate coupling to the flow above, must be added to the classical system of flow over an impermeable boundary.

In § 2 the model equations of motion, based on shallow-water approximations and the appropriate boundary conditions, are introduced. Finite-difference solutions of these equations are obtained and discussed in § 3, including a brief comparison with the experimental results of TML. Next, in § 4, box-model approximations are developed and compared to the shallow-water predictions. We present a summary of our results and some concluding remarks in § 5.

2. Formulation and shallow-water approximation

The configuration is sketched in figure 1. The driving force is the reduced gravity of the current, which is defined by

$$g' = (\rho_c - \rho_a)g/\rho_a, \tag{2.1}$$

where g is the acceleration due to gravity. For the rectangular case we use an $\{x, y, z\}$ Cartesian coordinate system with corresponding $\{u, v, w\}$ velocity components. We assume that the flow does not depend on the lateral coordinate y and that $v \equiv 0$. For the sector or full axisymmetric case we use a cylindrical coordinate system $\{r, \theta, z\}$ with corresponding $\{u, v, w\}$ velocity components. We assume that the flow does not depend on the angular coordinate θ and again that $v \equiv 0$.

We shall use a one-layer approximation. In the ambient fluid domain, of density ρ_a, we assume that $u = v = w = 0$ and hence this fluid is in purely hydrostatic balance. The motion is assumed to take place in the lower layer only, $0 \leqslant x \leqslant x_N(t)$ and $z \leqslant h(x, t)$. As in the classical inviscid shallow-water analysis of a gravity current,

we argue that the predominant vertical momentum balance is hydrostatic and that viscous effects in the horizontal momentum balance are negligibly small. Hence the motion is driven by the pressure and inertia forces in this horizontal direction. On the other hand, pressure continuity between the ambient and the current on the interface $z = h(x,t)$ indicates that the horizontal pressure gradient in the current is given by

$$\frac{\partial p}{\partial x} = \rho_a g' \frac{\partial h}{\partial x}. \tag{2.2}$$

These assumptions and the use of (2.2) simplify the momentum equations for the current. The next step is to consider the z-average of the equations of motion, which, in conjunction with volume continuity, produces a system of equations for $h(x,t)$ and for the averaged longitudinal velocity $u(x,t)$. However, at this stage it is useful to consider the contribution of the porous boundary to the expected flow, which is the major difference between the present situation and the classical one.

The porous boundary is conveniently incorporated into our analysis as a boundary condition for the vertical velocity component at the bottom, $w(x, z = 0, t)$, denoted w_b. This is of course equal to the rate of discharge through the porous substrate. TML (§ 4) developed a useful correlation for this variable which is expected to be valid when the Reynolds number of the flow through the porous medium, $Re' = w_b d/v$, is smaller than about 10; here d is the diameter of the pores. In this case, the employment of Darcy's law under the assumption that the porous layer has a constant thickness and the fluid above and below it is in vertical hydrostatic balance, yields (using dimensional variables)

$$w_b(x,t) = \frac{1}{\tau} h(x,t), \tag{2.3}$$

where τ is proportional to v/g' and also depends on the porous properties of the boundary. However, for a given configuration and with the effects of saturation of the pores and entrainment into the current excluded, τ is a constant.

Moreover, TML also showed that if τ is a constant on the entire boundary below the current then the condition (2.3) implies that the volume of the heavier fluid above the porous substrate decreases like $\exp(-t/\tau)$ (see § 2.2 below) in quite general circumstances of motion. This provides an efficient means for the experimental evaluation of τ for a given combination of fluid and boundary. TML made use of the expected exponential decay feature to evaluate the values of τ from measurements of the volume for the various settings used in their experiments. We shall elaborate on this issue in § 3.

Our present study adopts the condition (2.3) and assumes that the necessary value of τ is provided. We show that this is a sufficient condition for the incorporation of the porous-boundary effect in the shallow-water formulation. For simplicity and due to lack of further information, we assume that τ is a constant on the porous portion of the bottom boundary. If an impermeable portion is present (usually in the lock domain) the boundary condition there is $w(x, z = 0, t) = 0$ which can be treated as the limit $\tau \to \infty$ of (2.3). Furthermore, we show that if the given τ is a constant on the entire bottom boundary then simple box-model analytical approximations can be obtained.

This framework is, strictly speaking, specialized for the configurations of the type used by TML. Deviations from the present framework of assumptions may occur in practical circumstances. However, we suggest that many additional pertinent details, when available, can be incorporated in a straightforward extension of the analysis presented here by using τ as a function of x and of dependent variables of the current,

such as $h(x,t)$. A compatible practical situation is when a thin layer of low porosity separates fluid above and a thick high-porosity bed below (say, a layer of sand above gravel). Let l and Φ be the thickness and the porosity of the porous domain into which the gravity current drains. The portion of the porous region that is subjected to the influx with velocity w_b at its upper boundary is expected to reach saturation in the typical time interval $l\Phi/w_b$. If this time is substantially larger than the typical time of propagation of the gravity current, T, then the details of the flow in the porous bed are not expected to influence the flow of the current above the substrate. With the aid of (2.3) this condition can be expressed as $l\Phi/h_0 \gg \lambda$, where λ is the governing dimensionless parameter defined below, typically a small number. This condition is not very restrictive, but when it is violated the lateral flow in the region below the current may become important (i.e. the absorbed fluid is forced to move laterally rather than vertically) and a feedback flux may occur. In this case the present analysis needs augmenting, and the motion above and in the porous regions must be determined by coupled equations. Such problems were recently discussed by Davis & Hocking (1999) in the context of viscous spreading of liquids on a porous base.

Subsequently, the governing equations in the region of the current are averaged in z, and reduced to a system of equations for the position of the interface, $h(x,t)$, and for the z-averaged longitudinal velocity, $u(x,t)$. The difference from the classical current over an impermeable boundary is the presence of the non-zero vertical velocity on the boundary $z = 0$, for which we use (2.3).

It is convenient to scale the dimensional (denoted by the asterisks) variables as follows

$$\{x^*, h^*, t^*, u^*\} = \{x_0 x, h_0 h, T\, t, U u\}, \tag{2.4}$$

where

$$U = (h_0 g')^{1/2} \quad \text{and} \quad T = x_0/U. \tag{2.5}$$

Here h_0 and x_0 are the initial height and length of the current, U is a typical inertial velocity of propagation of the nose of the current and T is a typical time period for longitudinal propagation for a typical distance x_0. In the axisymmetric case x is replaced by r.

This scaling produces the non-dimensional parameter

$$\lambda = T/\tau \tag{2.6}$$

which simply reflects the ratio between the typical time of propagation of the nose to the typical time of descent of the interface due to the porosity of the boundary, the former over a length x_0 and the latter over a height h_0. This turns out to be the main parameter in the present analysis. It can be anticipated that the interesting cases have small values of λ, because otherwise the fluid has drained into the porous boundary before any significant propagation occurs. Indeed, for most of the experiments discussed by TML λ was in the range 0.02–0.24. The small value of λ in the TML experiments inhibits the rapid piling-up of a thick layer of salt water in the region below the porous grid, and hence prevents the formation of a significant gravity current in this region, in accordance with the assumption that this domain has a passive role.

The relevant Reynolds numbers can now be rewritten using the dimensionless variables as

$$Re = Re_0 \frac{\mathrm{d}x_N}{\mathrm{d}t} h_N \quad \text{and} \quad Re' = Re'_0 h, \tag{2.7}$$

where $Re_0 = g'^{1/2} h_0^{3/2}/\nu$ and $Re'_0 = \lambda g'^{1/2} h_0^{3/2} d/(x_0 \nu)$; here h_0, x_0 and d are dimensional.

This form is convenient for estimating the instantaneous importance of the viscous effects in the current and in the porous substrate in terms of the dimensionless results calculated below.

The equations of motion can be conveniently expressed either for h and the combined variable,

$$q = uh, \tag{2.8}$$

in 'conservation form', or for the original variables in 'characteristic form', as follows.

2.1. *The governing equations*

Consider first the rectangular case. In conservation form the equations can be written as

$$\frac{\partial h}{\partial t} + \frac{\partial}{\partial x}(uh) = -\lambda h \tag{2.9}$$

and

$$\frac{\partial}{\partial t}(uh) + \frac{\partial}{\partial x}[u^2 h + \tfrac{1}{2}h^2] = -\lambda uh. \tag{2.10}$$

In characteristic form this becomes

$$\begin{bmatrix} h_t \\ u_t \end{bmatrix} + \begin{bmatrix} u & h \\ 1 & u \end{bmatrix} \begin{bmatrix} h_x \\ u_x \end{bmatrix} = \begin{bmatrix} -\lambda h \\ 0 \end{bmatrix}. \tag{2.11}$$

Consider now the axisymmetric case. In conservation form the equations can be written as

$$\frac{\partial h}{\partial t} + \frac{\partial}{\partial r}(uh) = -\frac{uh}{r} - \lambda h \tag{2.12}$$

and

$$\frac{\partial}{\partial t}(uh) + \frac{\partial}{\partial r}[u^2 h + \tfrac{1}{2}h^2] = -\frac{u^2 h}{r} - \lambda uh, \tag{2.13}$$

which in characteristic form become

$$\begin{bmatrix} h_t \\ u_t \end{bmatrix} + \begin{bmatrix} u & h \\ 1 & u \end{bmatrix} \begin{bmatrix} h_r \\ u_r \end{bmatrix} = \begin{bmatrix} -uh/r - \lambda h \\ 0 \end{bmatrix}. \tag{2.14}$$

An unusual boundary condition which may appear in this problem is the presence of a non-porous section of the boundary, typically in the lock region $x \leqslant 1$. This is readily accounted for by setting $\lambda = 0$ in the equations of motion for the impermeable region. Actually, we note that λ can be allowed to vary with x and t without affecting the foregoing formulation. This may model motion over a boundary of complex structure and prone to partial saturation. However, this flexibility was not pursued further in the present work.

The velocity variable u at the origin is zero. In addition, a boundary condition for the velocity at the nose is essential for a proper physical definition and mathematical closure of the problem. The appropriate condition has been well studied, both theoretically and experimentally (Benjamin 1968; Huppert & Simpson 1980). The pertinent result is that

$$\frac{\mathrm{d}x_N}{\mathrm{d}t} = Fr(h_N)^{1/2}, \tag{2.15}$$

$$Fr = \begin{cases} 1.19 & (0 \leqslant h_N/\mathscr{H} \leqslant 0.075) \\ 0.5\mathscr{H}^{1/3} h_N^{-1/3} & (0.075 \leqslant h_N/\mathscr{H} \leqslant 1), \end{cases} \tag{2.16}$$

where $\mathscr{H}$ is the initial depth ratio of the ambient fluid to the current, or the thickness of the ambient layer scaled with h_0. In general, we consider $1 \leqslant \mathscr{H} < \infty$, but the more detailed calculations presented in this paper are for $\mathscr{H} = 1$, the same regime as the experiments of TML.

The boundary conditions for the interface height variable h can be incorporated by considering the characteristic paths and relationships (see Bonnecaze *et al.* 1993 for further discussion). The standard derivation, see for example Anderson, Tannehill & Pletcher (1984), requires first the determination of the eigenvalues of the matrix of coefficients, which are

$$l_{\pm} = u \pm \sqrt{h},$$

and the corresponding eigenvectors

$$(1, \pm\sqrt{h}).$$

Consequently, the relationships between the variables on the characteristics with $\mathrm{d}x/\mathrm{d}t = l$, are

$$l_{\pm} : \mathrm{d}h \pm \sqrt{h}\,\mathrm{d}u = -\lambda h\,\mathrm{d}t. \tag{2.17}$$

2.2. *The global volume balance*

Let $\mathscr{V}(t)$ denote the volume per unit width of the heavier fluid above the porous boundary. TMS showed that the correlation (2.3) between the velocity at the base and the local height leads, by purely kinematic considerations, to

$$\mathscr{V}(t) = \mathscr{V}(0)\mathrm{e}^{-\lambda t}. \tag{2.18}$$

However, this simple and apparently robust result is based on the assumption that the porous boundary starts at the origin. In relevant practical circumstances, and also in the experiments performed by TMS, this condition is not fulfilled: the porous boundary actually extends only for $x > 1$, while the portion $0 \leqslant x \leqslant 1$ is impermeable.

For the sake of completeness we shall briefly rederive the result (2.18) in the context of the shallow-water theory, using (2.9) and (2.12) and the boundary conditions $u = 0$ at the origin.

In the rectangular case

$$\mathscr{V}(t) = \int_0^{x_N(t)} h(x,t)\,\mathrm{d}x, \tag{2.19}$$

and hence

$$\frac{\mathrm{d}\mathscr{V}}{\mathrm{d}t} = \int_0^{x_N(t)} \frac{\partial h}{\partial t}\,\mathrm{d}x + \frac{\mathrm{d}x_N}{\mathrm{d}t} h_N. \tag{2.20}$$

On the other hand, integration of (2.9) yields

$$\int_0^{x_N(t)} \frac{\partial h}{\partial t}\,\mathrm{d}x = -u(x = x_N)h_N - \lambda \int_0^{x_N(t)} h(x,t)\,\mathrm{d}x. \tag{2.21}$$

Combining (2.20) and (2.21) and using (2.19), we obtain

$$\frac{\mathrm{d}\mathscr{V}}{\mathrm{d}t} = -\lambda\mathscr{V}, \tag{2.22}$$

which proves (2.18). Note that in dimensionless form $\mathscr{V}(0) = 1$.

In the axisymmetric case

$$\mathscr{V}(t) = \int_0^{r_N(t)} h(r,t) r\,\mathrm{d}r, \tag{2.23}$$

and hence

$$\frac{\mathrm{d}\mathscr{V}}{\mathrm{d}t} = \int_0^{r_N(t)} \frac{\partial h}{\partial t} r \,\mathrm{d}r + r_N \frac{\mathrm{d}r_N}{\mathrm{d}t} h_N. \tag{2.24}$$

We eliminate $\partial h/\partial t$ with the aid of (2.12) and, after some rearrangement, we again obtain the result (2.22). Note that in dimensionless form $\mathscr{V}(0) = \frac{1}{2}$.

If the portion $x \leqslant 1$ is non-porous, the lower limit of the integral on the right-hand side of (2.21) is 1, and instead of (2.22) we obtain

$$\frac{\mathrm{d}\mathscr{V}}{\mathrm{d}t} = -\lambda \left[1 - \frac{\mathscr{V}_1(t)}{\mathscr{V}(t)}\right] \mathscr{V}, \tag{2.25}$$

where $\mathscr{V}_1$ is the volume of the current above the non-porous boundary. In the initial stages of propagation the ratio $\mathscr{V}_1/\mathscr{V}$ is close to 1 and hence considerable deviation from the exponential decay is expected, and, overall, the apparent rate of decay is smaller than in the idealized case.

The discrepancy between (2.22) and (2.25) is very important for larger values of λ. However, even for the parametric range in the experiments of TML this effect seems to be relevant. TML fitted their measurements, performed for a boundary with a non-porous section in the lock region, to (2.18) as a means for determining the value of λ (and actually of τ because the other quantities which enter (2.6) were prescribed). We claim that this procedure underestimates the values of λ (overestimates the values of τ). The calculations presented in the next section indicate that the values of τ were overestimated by about 35% (for the single grid substrate).

3. Numerical results

The governing equations (2.9)–(2.10) and (2.12)–(2.13) were formulated in conservation form for the variables h and $q = uh$. Following closely the approach of Bonnecaze *et al.* (1993, 1995) and Ungarish & Huppert (1998), we obtained the numerical solutions using a finite-difference two-step Lax–Wendroff method. To facilitate the implementation of the boundary conditions, the longitudinal coordinate x (or r) was mapped into $y = x/x_N(t)$, which maintains the current in the domain $0 \leqslant y \leqslant 1$. Consequently the original equations were subjected to the modifications

$$\left(\frac{\partial}{\partial t}\right)_x = \left(\frac{\partial}{\partial t}\right)_y - y\frac{\dot{x}_N}{x_N}\left(\frac{\partial}{\partial y}\right)_t \quad \text{and} \quad \left(\frac{\partial}{\partial x}\right)_t = \frac{1}{x_N}\left(\frac{\partial}{\partial y}\right)_t, \tag{3.1}$$

where the subscript denotes the fixed variable and the dot differentiation with respect to time. In order to suppress oscillations of numerical origin a small artificial viscosity term, of the form $-b\,\partial[\alpha h(\partial u/\partial x)]/\partial x$, was added to the left-hand side of the momentum equation (2.10). Here $\alpha = (|u| + h^{1/2})\Delta x$, where Δx is the mesh interval, and $b = 0.15$ were used. Numerical tests indicated that this artificial term affected the distance of propagation by less than 1% in the cases presented below.

The initial conditions used were

$$h = 1 \quad \text{and} \quad u = 0 \quad (0 \leqslant y \leqslant 1, t = 0) \tag{3.2}$$

and

$$x_N = 1 \quad (t = 0), \tag{3.3}$$

while the boundary conditions used were

$$u = 0 \quad (y = 0) \tag{3.4}$$

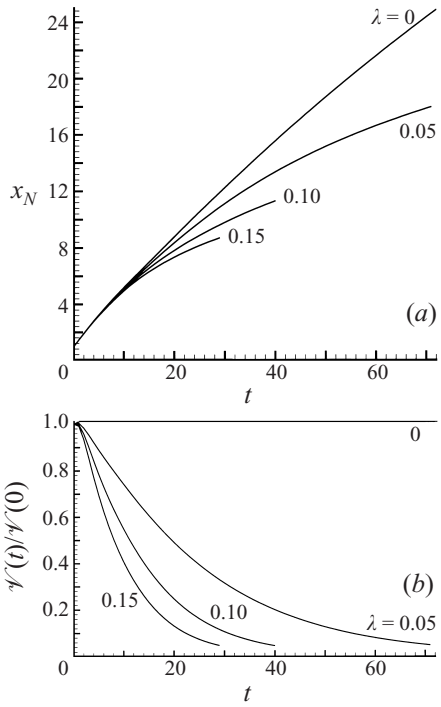

FIGURE 2. Rectangular gravity current: numerical shallow-water model calculations of x_N and $\mathscr{V}(t)/\mathscr{V}(0)$ as functions of t for various values of λ. The $\lambda > 0$ cases stopped when the volume reached about 0.05 of initial value.

and

$$u = Fr[h(y = 1, t)] \times [h(y = 1, t)]^{1/2} \quad (y = 1), \tag{3.5}$$

with the values of Fr prescribed by (2.16). The boundary conditions for h at $y = 0$ and $y = 1$ must be calculated, for each time step, from the balances on the characteristics $l_{\pm}$.

The numerical computations presented here are for $\mathscr{H} = 1$, i.e. the initial heights of the heavy current fluid and of the lighter ambient fluid are equal. This was also the setup in the experiments of TML.

Figures 2 and 3 give a quick insight into the influence of the parameter λ on the propagation distance and volume decay in configurations with an impermeable boundary in the lock region $x \leqslant 1$ (or $r \leqslant 1$). The porosity has little influence on the propagation during an initial period ($t < 12$ in the rectangular case and $t < 8$ in the axisymmetric case). The explanation for this is given below. Afterwards, the porosity slows the current down and shortens the effective distance of propagation. It is evident that these effects become more pronounced as the parameter λ increases. Computations with non-zero λ were stopped when either of the following conditions was achieved: the volume decreased to 5% of the initial value, or h_N became smaller than 0.01. There were indications of fast accumulation of numerical errors afterwards. The thickness of the cylindrical current is expected to decrease as the square of the distance and hence for this geometry the condition on h_N tends to be fulfilled sooner than the condition on the volume. The volume $\mathscr{V}(t)/\mathscr{V}(0)$ decreases slower than $\mathrm{e}^{-\lambda t}$ because of the presence of the non-porous portion of the boundary. This feature is also discussed further below.

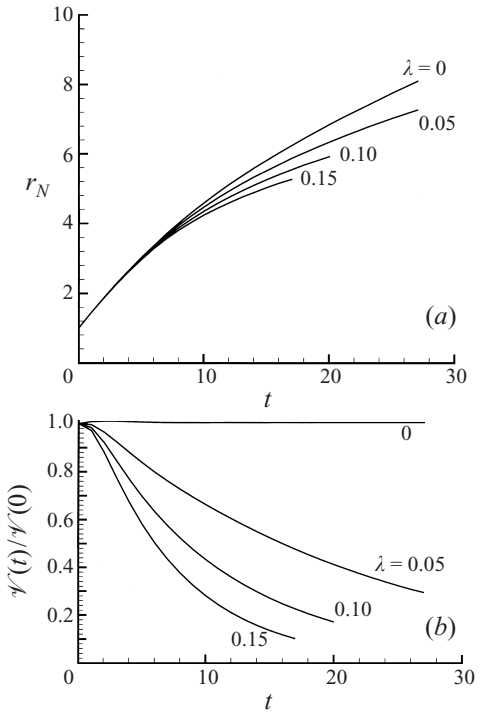

FIGURE 3. Axisymmetric gravity current: numerical shallow-water model calculations of r_N and $\mathscr{V}(t)/\mathscr{V}(0)$ as functions of t for various λ. The $\lambda > 0$ cases stopped when $h_N \approx 0.01$.

More detailed results for the shallow-water equations in a rectangular configuration are presented in figures 4–6 using a numerical grid of 200 points and with a time step of 5×10^{-3}. In all cases the initial depth ratio is $\mathscr{H} = 1$. Three cases are presented for comparison: case I is a classical current over an impermeable boundary ($\lambda = 0$); in case II $\lambda = 0.1$ and the porous region extends for $x > 1$; and in case III $\lambda = 0.1$ and the porous region starts at the origin.

In the initial stages of the motion, for $t < 15$, and in particular for $t < 5$, the qualitative behaviour of the interface is similar in the three cases. As expected, the fluid initially collapses from the front to $h_N \approx 0.6$. In the classical ($\lambda = 0$) case this head height persisted for a while ($t < 3$), during which time the speed of propagation is constant. The porosity causes a continuous decrease of h_N, as expected. After the adjustment time $t \approx 15$ the classical $\lambda = 0$ current tends to approach the similarity form of solution with a head-up, tail-down smooth profile and with u a linear function of x. Here the porosity tends to strengthen the differences between the head and the tail regions, especially in case II where u becomes a non-monotonic function of x. Quantitatively, up to $t \approx 10$ the distance of propagation is almost the same in all three cases, despite the fact that the height of the nose decreases considerably more in the porous cases ($h_N = 0.162, 0.092, 0.076$ at $t = 10$ in cases I, II, and III, respectively). The reason is the behaviour of Fr with h_N, cf. (2.16), which makes the velocity of propagation a weak function of h_N ($\mathrm{d}x_N/\mathrm{d}t \propto h_N^{1/6}$). In the deep stage of propagation, $h_N < 0.075$, the porous drainage has a significant influence on the velocity of propagation: at $t = 40$ the non-porous x_N is about 50% larger than for the porous cases.

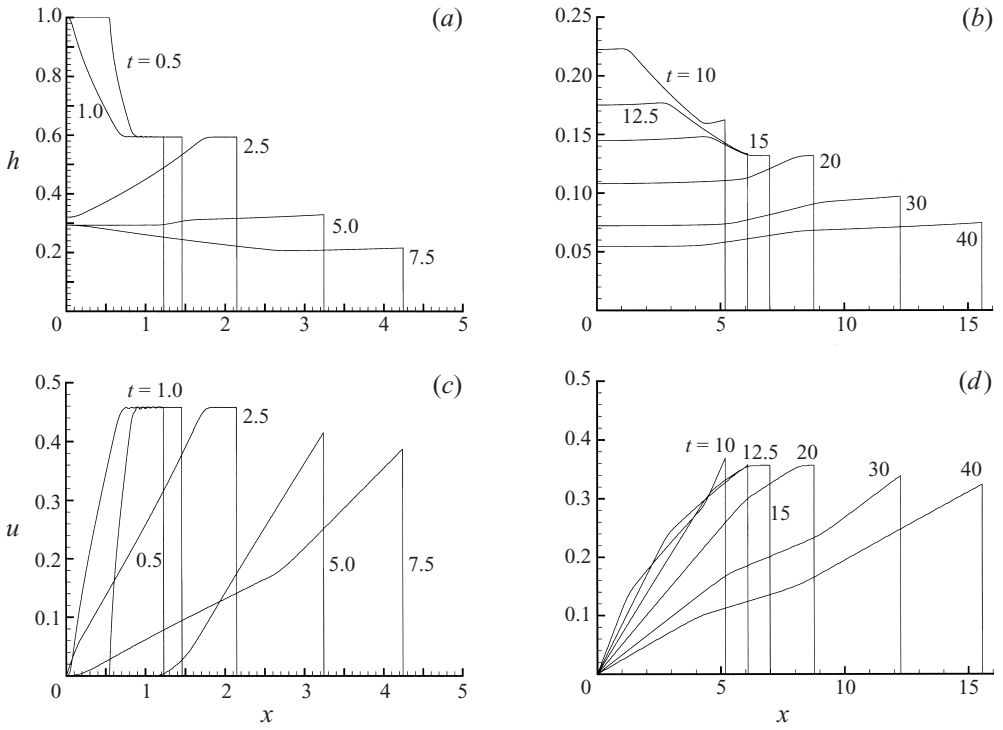

FIGURE 4. Rectangular gravity current: numerical shallow-water model calculations of case I, with an impermeable wall ($\lambda = 0$). (*a*) and (*b*) h as a function of x at various t; (*c*) and (*d*) u as a function of x at various t.

Comparing cases II and III we notice that the non-porous portion $x < 1$ keeps the fluid at a higher level than in the tail which follows the head. In addition, the overall volume in case II is higher (by $48\%, 81\%, 110\%$ at $t = 10, 20, 30$) than the $e^{-\lambda t}$ behaviour in case III, and therefore the propagation is slightly faster.

Similar results of the shallow-water equations in the axisymmetric configuration are presented in figures 7–9. Three cases are again presented for comparison: case I is a classical current over an impermeable boundary ($\lambda = 0$); in case II $\lambda = 0.1$ and the porous region extends for $r > 1$; and in case III $\lambda = 0.1$ and the porous region starts at the origin. The qualitative behaviour is as in the rectangular case, but the reduction of h_N is proportional to r_N^2. Some oscillations appear near the centre for $t > 5$ which seem to be introduced by the reflection (from the axis) of the initially backward-moving wave created at $t = 0$ at the collapsing front, as also discussed by Bonnecaze *et al.* (1995, § 3.1). In this respect the axisymmetric current (over a solid boundary) is different from the rectangular one: although the same initial collapse of the front to $h_N \approx 0.6$ occurs in both cases, the subsequent propagation with a constant velocity and a constant h_N is not possible in the diverging cylindrical geometry, and therefore a deceleration of the head domain occurs, accompanied by the appearance of a positive $\partial h/\partial r$ and a non-monotonic profile of u as a function of r. The porous drainage tends to amplify these oscillations, and it is difficult to decide if this is a numerical perturbation or an indication of a physical instability. However, since the amount of fluid in the relevant region is relatively small this is not expected to be of significance to the propagating current.

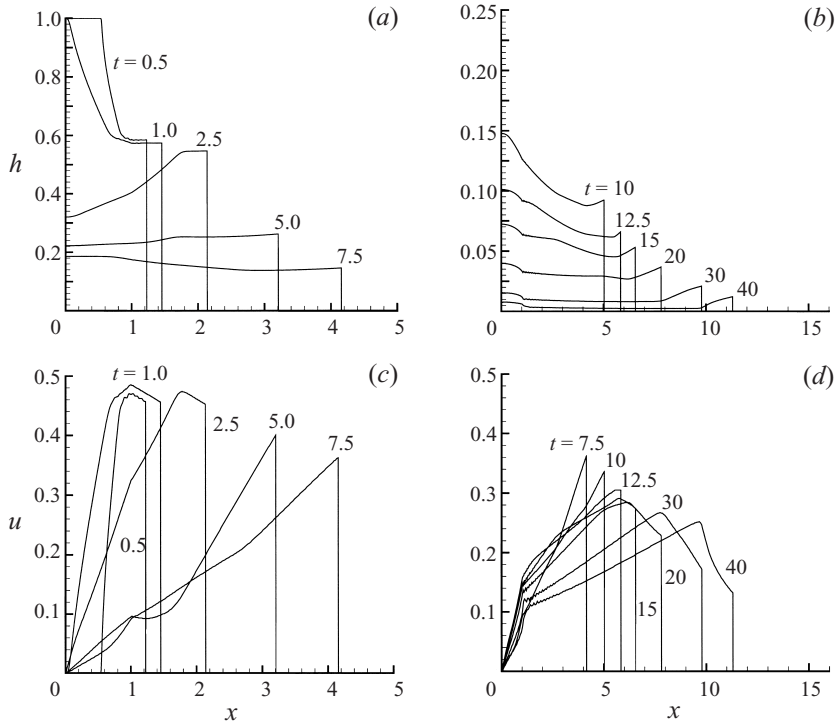

FIGURE 5. As figure 4 but for case II with $\lambda = 0.1$ for $x > 1$ and an impermeable wall for $x \leqslant 1$.

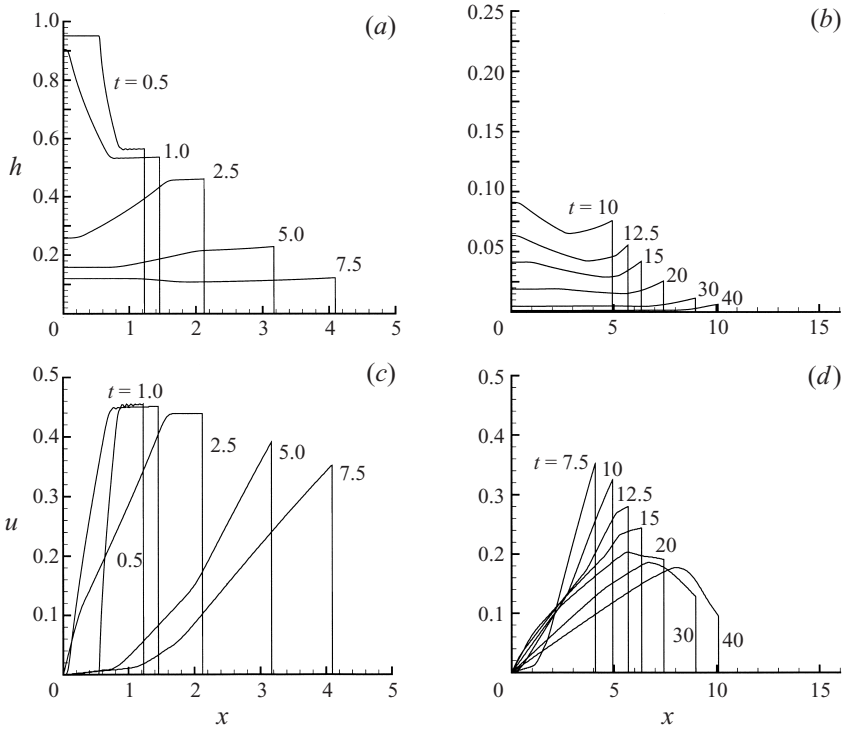

FIGURE 6. As figure 4 but for case III with $\lambda = 0.1$ for $x > 0$.

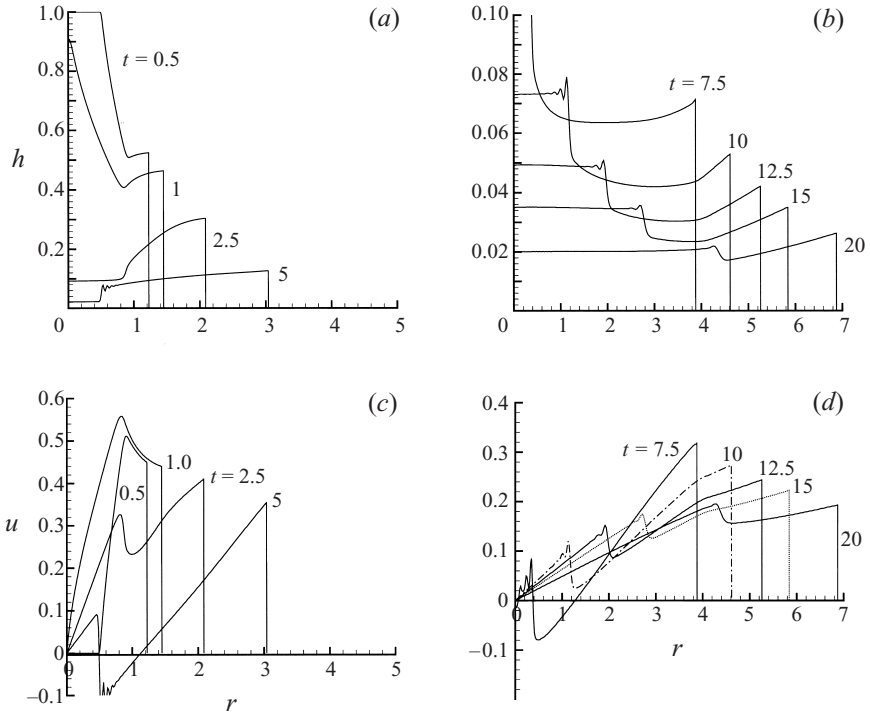

FIGURE 7. Axisymmetric gravity current: numerical shallow-water model calculations of case I with an impermeable wall ($\lambda = 0$). (*a*) and (*b*) h as function of r at various t; (*c*) and (*d*) u as a function of r at various t.

3.1. *Comparisons with the experiments of TML*

Detailed comparisons with the experiments of TML are beyond the scope of the present study. However, some insights into the process and additional confidence in the theory may be gained by a discussion of the numerical results for the main parameters used in the experiment.

The major input needed for a proper comparison is the value of τ which, in the present theory, is expected to be provided by (special) experiments. Indeed, TML determined values of τ, and we first apply our numerical code to verify the accuracy of the procedure and to suggest 'corrected' values of τ. Subsequently, using these corrected values we calculate $x_N(t)$ for several experimental cases.

The procedure of TML for evaluating τ was essentially as follows. They released a current of known properties in the experimental tank and recorded its volume $\mathscr{V}$ as a function of t. The experimental values $\mathscr{V}(t)/\mathscr{V}(0)$ were used to fit the approximation $\mathrm{e}^{-t/\tau_{TML}}$ (with the subscript TML denoting the values obtained by this procedure), where τ_{TML} was determined so that the correspondence was 'good'.

The problem with this procedure is that the exponential decay of $\mathscr{V}$ with t is strictly valid only when the entire bottom boundary beneath the current is porous, while in the experimental tank the initial lock region, $0 \leqslant x \leqslant 1$, was impermeable. As indicated in § 2.2 the apparent (fitted) rate of decay of λ is smaller (the apparent (fitted) τ is larger) than the correct value of the system. Moreover, the scatter of the data around the fitted curve is expected to contain a systematic component in addition to the random contributions of measurement errors (figure 7 of TML seems to confirm

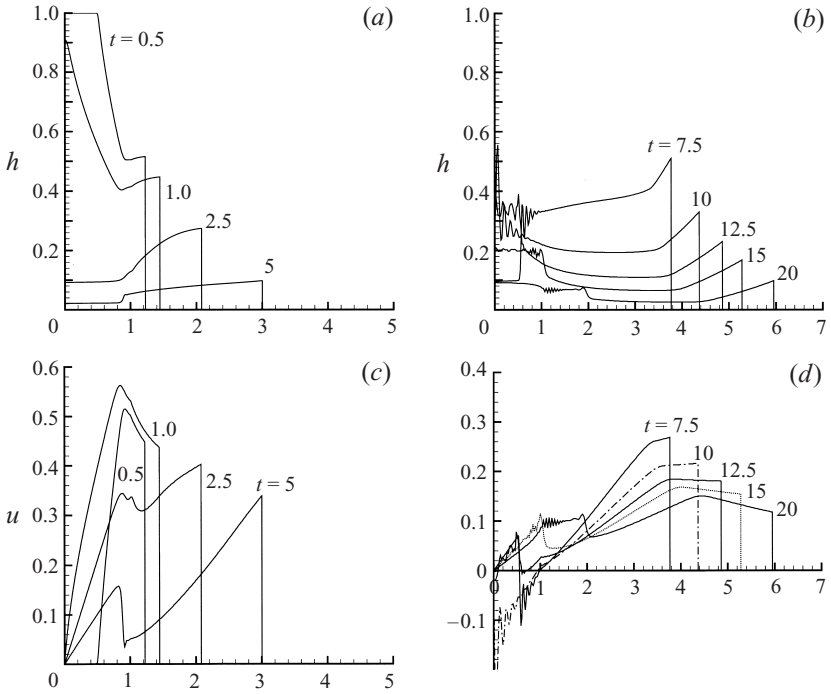

FIGURE 8. As figure 7 but for case II with $\lambda = 0.1$ for $r > 1$ and impermeable wall for $r \leqslant 1$.

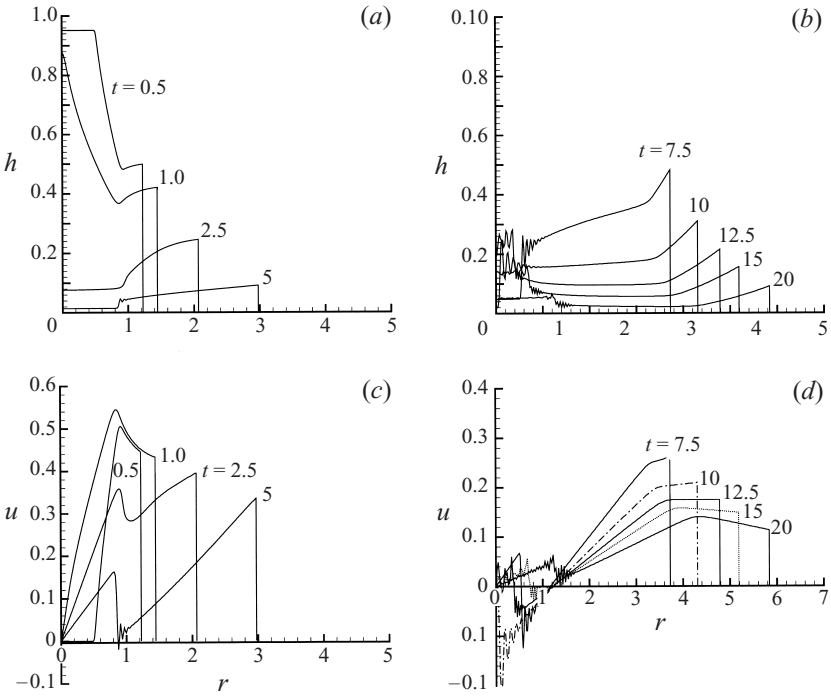

FIGURE 9. As figure 7 but for case III with $\lambda = 0.1$ for $r > 0$.

g' (cm s^{-2})	9.8	49	98
τ (s)	12.30	4.32	2.19
τ_{TML} (s)	17.57	6.53	3.52

TABLE 1. Values of τ for different g' corresponding to the TML experiments on a simple grid: corrected and reported (subscript TML).

this observation). TML were aware of this difficulty (private communication) and attempted to overcome it by discarding initial time readings in the fitting of τ. This approach is indeed expected to reduce the contribution of the impermeable portion, but does not compensate for the effect; moreover, the later measurements of the volume are prone to larger experimental errors owing to mixing effects.

To assess and perhaps improve the experimental values of τ_{TML} we solved the following 'inverse' problem: for the parameters g' and x_0 of the experiment, find the 'correct' value of τ so that the resulting (numerical) values of $\mathscr{V}(t)/\mathscr{V}(0)$ are 'well fitted' by an exponential decay with the value τ_{TML} reported for this experiment. (Inspired by an inspection of figure 8 of TML, we defined 'well fitted' as a collocation at the time when $\mathscr{V}/\mathscr{V}(0) = 0.3$). The results of the inverse problem are given in table 1, together with the values of TML.

The 'correct' τ are 30–38% smaller than the apparent ones. We also note that the 'correct' values of τ are closer to the theoretical proportionality to g'^{-1} than the values reported by TML. The deviation is more pronounced for the larger value of τ (smaller value of g') and we speculate that this is a result of remixing with fresh water. Indeed, remixing reduces the effective g', and for smaller g' there is more time for remixing during the process.

Figure 10 illustrates these results: for $x_0 = 15$ cm, $h_0 = 20$ cm and $g' = 9.8, 49, 98$ cm s^{-2} the points are numerical calculations of $\mathscr{V}/\mathscr{V}(0)$ with the 'correct' values of τ, while the curves are the exponential decay using the τ_{TML} values. On the other hand, tests (not shown here) indicate that the direct use of the τ_{TML} values as the 'correct' ones in the numerical simulations yield discrepancies of order tens of percent in the behaviour of $\mathscr{V}(t)$ as compared to the exponential decay with the same τ_{TML}.

Figure 11 displays results of our computations corresponding to the experiments of TML with variables given in table 2. The results are presented in the rescaled form used in figure 9 of TML, i.e. in the present notation $(x_N - 1)\lambda_{TML}$ vs. $\lambda_{TML}t$ on a log-log plot. The computations were performed with the values of λ (or τ) inferred as the 'correct' ones (see table 1). The fifth column of table 2 indicates the practical limit on the rescaled range of propagation that could be followed in the finite experimental tank. The last column vindicates the use of an inviscid approximation. The penultimate column may indicate that the validity of Darcy's law in the pores is questionable in the initial part of the motion, in particular for the current with $g' = 98$ cm s^{-2}; however, we keep in mind that the flow through the pores slows down like h, which is on the average faster than the relative increase of the length $x_N(t)$.

The behaviour depicted in figure 11 is consistent with that presented by TML for their experiments with exceptions for small and large values of $\lambda_{TML}t$, which can be attributed to experimental errors and the influence of the far endwall of the container. There is, however, one remarkable difference: the experimental curve for $\lambda = 0.382$ undergoes a drastic slope reduction and intersects the other curves in $1 < \lambda_{TML}t < 3$, then regains the large slope. We have no explanation for this discrepancy.

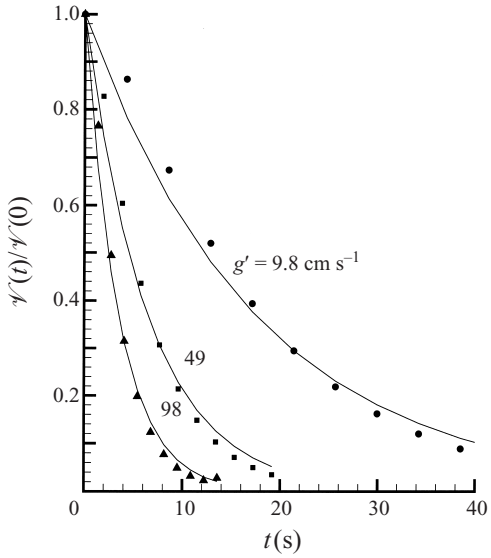

FIGURE 10. The dimensionless volume $\mathscr{V}(t)/\mathscr{V}(0)$ as a function of time (in s) for the configurations of the TML experiments with $x_0 = 15$ cm, $h_0 = 20$ cm and $g' = 9.8, 49, 98$ cm s^{-2} determined by the numerical shallow-water model calculations performed with the corrected values of τ (symbols), and the curves display $\exp(-t/\tau_{TML})$, see table 1. (The values in the computations are $\lambda = 0.087$, 0.111, 0.155, and for the curves $\lambda_{TML} = 0.061$, 0.073, 0.097.)

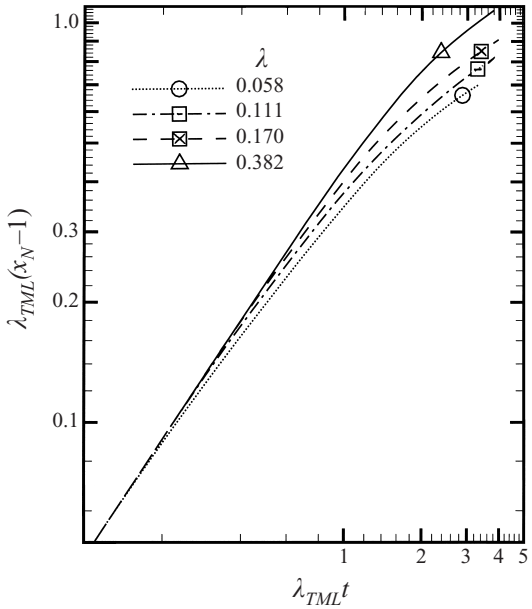

FIGURE 11. Distance of propagation as function of time (in rescaled forms) simulated by numerical shallow-water model calculations for the data of table 2.

We conclude that there seems to be fair overall agreement between the present shallow-water theory and the experiments of TML. However, a detailed and thorough comparison with experimental data is beyond the scope of this paper and would require additional experiments.

g' (cm s^{-2})	x_0 (cm)	λ	λ_{TML}	$(L_{\max}/x_0)\lambda_{TML}$	Re'_0	Re_0
9.8	10	0.058	0.041	0.80	8	3×10^4
49	15	0.111	0.073	0.95	23	6×10^4
49	23	0.170	0.113	0.96	23	6×10^4
98	37	0.382	0.237	1.27	45	9×10^4

TABLE 2. Data for comparison with the experiments of *TML*. g' and x_0 are variables of the experiment, $L_{\max} = 195$ cm is the length from the gate of the lock to the opposite wall. λ_{TML} and λ are calculated with τ_{TML} and τ given in table 1.

For the axisymmetric configuration there are no available experimental data, to the best of our knowledge, and hence no comparisons can be attempted.

4. Box-model approximations

Box models have been successfully used for quick estimates of the global behaviour of gravity currents in various circumstances. Here we develop this type of approximation for the problem under investigation and assess its validity via comparisons with the shallow-water numerical results for typical values of λ.

The current is viewed as a control volume of rectangular cross-section, i.e. height $h_N(t)$ and length $x_N(t)$ ($r_N(t)$ in the axisymmetric case). For simplicity we assume that the porous floor starts at the origin.† The changes of this control volume with time, which are expected to reproduce the motion of the gravity current, are governed by the following considerations: (*a*) the volume balance (2.18); and (*b*) the nose-propagation correlation, or Froude condition, (2.15)–(2.16). The initial conditions for x_N and h_N are known, as is the value of the initial depth ratio, $\mathscr{H}$.

In the limit $\lambda \to 0$ the box model for the impermeable wall is recovered, as described in the Appendix.

4.1. *Rectangular geometry*

The volume balance (2.18) is expressed as

$$x_N(t)h_N(t) = \mathrm{e}^{-\lambda t}, \tag{4.1}$$

and the nose Froude condition can be written

$$\frac{\mathrm{d}x_N}{\mathrm{d}t} = Frh_N^{1/2}. \tag{4.2}$$

The initial conditions are

$$x_N = 1 \quad \text{and} \quad h_N = 1 \quad (t = 0). \tag{4.3}$$

We distinguish between the shallow stage, $0 \leqslant t \leqslant t_*$, during which Fr varies with h_N, and the deep stage, $t > t_*$, during which $Fr = 1.19$.

† When a non-porous portion is incorporated the solution requires numerical integration of ordinary differential equations. The details will be given in a separate paper.

The shallow stage appears only if the initial depth ratio $\mathscr{H} < 1/0.075$. For this case, we substitute $Fr = (\frac{1}{2})\mathscr{H}^{1/3}h_N^{-1/3}$ in (4.2) and eliminate h_N with the aid of (4.1). We obtain a differential equation for $x_N(t)$, which can be easily integrated to yield

$$x_N(t) = \left[\frac{7}{2\lambda}\mathscr{H}^{1/3}(1 - \mathrm{e}^{-\lambda t/6}) + 1\right]^{6/7} \qquad (t \leqslant t_*), \tag{4.4}$$

and with the use of (4.1),

$$h_N(t) = \mathrm{e}^{-\lambda t}/x_N(t). \tag{4.5}$$

The shallow stage terminates at the time t_* when $h_N(t_*) = 0.075\mathscr{H}$. By virtue of (4.5) and (4.4), and after some algebra, we can formulate this condition as

$$\frac{2}{7\mathscr{H}^{1/3}}\lambda\left(\frac{1}{0.075\mathscr{H}}\right)^{7/6} s^7 + s - 1 - \frac{2}{7\mathscr{H}^{1/3}}\lambda = 0, \tag{4.6}$$

where

$$s = \mathrm{e}^{-\lambda t_*/6}. \tag{4.7}$$

The numerical solution of this equation shows that t_* decreases when λ and/or $\mathscr{H}$ increases. This is expected: a larger λ causes a quicker decay to the deep stage and a larger $\mathscr{H}$ means that the current is initially closer to the deep stage. We denote by x_* the value of x_N at t_*. For the sake of a unified treatment, when $\mathscr{H} \geqslant 1/0.075$ and the shallow stage does not occur we define $t_* = 0$ and $x_* = 1$.

For the deep stage of propagation we substitute $Fr = 1.19$ in (4.2) and eliminate h_N with the aid of (4.1). We obtain again an equation for $x_N(t)$, which can be easily integrated to yield

$$x_N(t) = \left[3 \times 1.19\frac{1}{\lambda}(\mathrm{e}^{-\lambda t_*/2} - \mathrm{e}^{-\lambda t/2}) + x_*^{3/2}\right]^{2/3} \qquad (t \geqslant t_*) \tag{4.8}$$

with the height of the current given by (4.5).

After obtaining h_N, the instantaneous Reynolds number of the current can be readily evaluated by using (2.7): $Re = Re_0 Fr h_N^{3/2}$, where again distinction between the shallow and deep stages is necessary. We recall that transition to the viscous domain is expected to occur at $Re = 50$, where the preceding results become invalid. An analysis for the viscous domain is at present in progress and will be published in a separate paper.

We now compare the present box-model results to the simple model for the propagation of the current suggested by TML, equation (4.10) in their paper. In the present notation, that equation reads

$$x_N(t) = \frac{1}{\lambda}(1 - \mathrm{e}^{-\lambda t/2}) + 1 \tag{4.9}$$

(the last term does not actually appear in the paper TML, apparently due to a misprint, and the constant C of the paper has been set equal to 0.5, consistent with other results in that paper. Recall that TML consider $\mathscr{H} = 1$). Evidently, there are significant qualitative discrepancies between the models, although expansions for small values of t yield the same leading terms, $1 + (\frac{1}{2})t$, for both (4.4) and (4.9). The next terms in the expansions, however, are $-(1 + 2\lambda)t^2/48$ and $-\lambda t^2/8$, respectively. For $\lambda < 0.25$, (4.4) predicts a slower initial propagation than (4.9), but eventually this trend is reversed. The model suggested by TML does not distinguish between the shallow and deep stages of propagation.

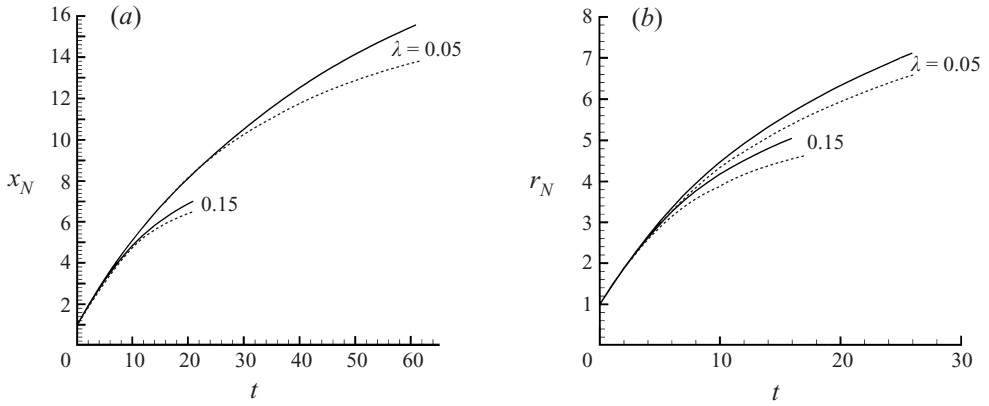

FIGURE 12. Shallow-water (solid, i.e. upper, lines) and box-model (dotted, i.e. lower, lines) calculations for propagation as function of t for two values of λ in (a) rectangular case; (b) axisymmetric case. The porous boundary starts at the origin.

It is interesting to note that the motion in the deep stage predicted by the present box model reflects an instantaneous balance between the total buoyancy force per unit width, $F_g \sim \rho g' h^2$, and the total inertial force per unit width, $F_i \sim \rho U^2 h$ (in dimensional form); where the symbol $\sim$ implies an order of magnitude relationship. Huppert (1982, Appendix A) used such balances to obtain simple estimates of the flow properties and the criteria describing transition between different flow regimes. Here, upon combining the balance $F_i \sim F_g$ with the volume balance, letting $U \sim \mathrm{d}x_N/\mathrm{d}t$ and using the initial condition $x_N(0) = 1$, we obtain, in dimensionless form,

$$x_N(t) \sim \left[\frac{3}{\lambda}(1 - \mathrm{e}^{-\lambda t/2}) + 1\right]^{2/3} \quad (t \geqslant 0), \tag{4.10}$$

a result very close to (4.8) for the case of an initially deep current.

A comparison between the predicted propagation by the present box model results and those obtained by the shallow-water equations for two values of λ is shown in figure 12(a) (from release point until decrease of volume to 5%). The agreement is good. The box-model approximation predicts a slower propagation than the shallow-water equations. This could be anticipated because in the shallow-water (and also real) profiles the value of h_N becomes quickly larger than the average h and hence the velocity of the nose is larger than that obtained under the assumption that h_N equals the average h.

4.2. *Cylindrical (axisymmetric) geometry*

The volume balance (2.18) is expressed as

$$r_N^2(t) h_N(t) = \mathrm{e}^{-\lambda t}, \tag{4.11}$$

and the nose Froude condition reads

$$\frac{\mathrm{d}r_N}{\mathrm{d}t} = Fr h_N^{1/2}. \tag{4.12}$$

The initial conditions are

$$r_N = 1 \quad \text{and} \quad h_N = 1 \quad (t = 0). \tag{4.13}$$

We proceed as for the rectangular case. Now, using (4.11), we obtain

$$h_N(t) = \mathrm{e}^{-\lambda t}/r_N^2, \tag{4.14}$$

and we also determine that in the shallow stage

$$r_N(t) = \left[4\frac{1}{\lambda}\mathscr{H}^{1/3}(1-\mathrm{e}^{-\lambda t/6})+1\right]^{3/4} \qquad (t \leqslant t_*), \tag{4.15}$$

where, again, t_* is the time when h_N reaches the value $0.075\mathscr{H}$, and is given by the solution of

$$\frac{1}{4\mathscr{H}^{1/3}}\lambda\left(\frac{1}{0.075\mathscr{H}}\right)^{2/3}s^4+s-1-\frac{1}{4\mathscr{H}^{1/3}}\lambda=0, \tag{4.16}$$

where

$$s = \mathrm{e}^{-\lambda t_*/6}. \tag{4.17}$$

As in the rectangular case, the solution of this equation indicates that t_* decreases when λ and/or $\mathscr{H}$ increase. For a prescribed combination of λ and $\mathscr{H}$ the axisymmetric current attains the deep stage in shorter time and distance of propagation than the rectangular current because its thickness decreases with the square of the distance.

Denote by r_* the value of r_N at t_*. For the sake of a unified treatment, when $\mathscr{H} \geqslant 1/0.075$ and the shallow stage does not occur, we define $t_* = 0$ and $r_* = 1$.

For the subsequent deep stage of propagation we obtain

$$r_N(t) = \left[4\times 1.19\frac{1}{\lambda}(\mathrm{e}^{-\lambda t_*/2}-\mathrm{e}^{-\lambda t/2})+r_*^2\right]^{1/2} \qquad (t \geqslant t_*). \tag{4.18}$$

As in the rectangular case, the motion in the deep stage predicted by the present box model reflects an instantaneous balance between the total buoyancy force, $F_g \sim \rho g' h^2 r_N$, and the total inertial force, $F_i \sim \rho U^2 h r_N$ (in dimensional form).

A comparison between the predicted propagation in axisymmetric circumstances of the present box-model results to those obtained by the shallow-water equations for two values of λ is shown in figure 12(b) (from the release point until decrease of the numerical h_N to 0.01). The agreement is good. As for the rectangular case, the box-model approximation predicts a slower propagation than the shallow-water equations.

5. Concluding remarks

In this paper we have analysed the behaviour of an inviscid lock-released gravity current which propagates over a horizontal porous boundary in either a rectangular or an axisymmetric geometry. The effect of this boundary was described by means of a parameter λ, which represents the ratio of the typical time of porous drainage, τ, to that of horizontal spread, $x_0/(h_0 g')^{1/2}$. The value of τ was assumed to be known for the fluid–boundary combination under simulation. The interesting cases correspond to small values of λ, otherwise the current is drained before any significant propagation can occur.

We formulated and solved the one-layer shallow-water equations for this problem, and pointed out the differences with the classical current (over an impermeable boundary). We compared the motion over an entire porous boundary and over one for which the portion under the lock is impermeable. We showed that the decrease of volume in the latter case deviates considerably from the exponential decay pointed out by TML

for the former case. This suggests that the evaluations of τ performed by TML from the measurements of volume fitted to the exponential decay curve must be adjusted downwards by typically 35%. Furthermore, because of the problematic contribution of the non-porous boundary beneath the lock region to the experimental finding of τ from lock-release experiments, we suggest a different method, as follows. If we let the heavy fluid 'settle' through an entire porous boundary (without performing any vertical motion) under external conditions of the ambient fluid pertinent to the gravity current of interest, the volume decay is expected to be exponential and conveniently given by the height of the interface between the two fluids, thus allowing a more accurate evaluation of τ. This may require a special mechanism for turning on and off the holes in the grid (in other words, instead of the vertical lock mechanism some kind of horizontal lock is needed to allow control on the start of the drainage of the current).

A brief comparison of shallow-water simulations with some experimental results of TML shows consistency in most cases. However, a detailed comparison between the theory and experiments, in particular for axisymmetric configurations, calls for a special study requiring additional experiments.

We developed box-model approximations which yield the distance of propagation and average thickness as explicit functions of time, in fair agreement with the shallow-water results.

The assumption of a constant λ in the porous domain of the boundary is an oversimplification for practical cases, but is not a necessary one. Formally, it can be readily relaxed in both the shallow-water and box-model approximation. Since the shallow-water equations are solved numerically, a quite complicated dependence of the vertical velocity at the base, w_b, see (2.3), on x, t and other variables (which will result in a similarly complicated λ) can be straightforwardly incorporated into the shallow-water analysis. For the box model it may become necessary to integrate the ordinary differential equations numerically when a variable λ is used. Practically, however, the employment of an improved representation of λ depends on the availability of more sophisticated models and data for the behaviour of a porous substrate. Indeed, the correlation suggested by TML and adopted in this work has not yet been tested, to our knowledge, on real porous materials. This topic requires investigation.

For very small values of λ the current propagates for much more than its initial length. Such a propagation, in the absence of porous drainage, would cause the current to approach a similarity form of behaviour. It is plausible that small λ will introduce only a small perturbation to this ideal similarity feature for a significant period of time; such a feature was indeed detected for the particle-driven current by Hogg, Ungarish & Huppert (2000), which allowed a convenient asymptotic expansion to be obtained. This investigation is in progress and will be published in a separate paper.

There is an intuitive similarity between a homogeneous current over a porous wall and a particle-driven current over an impermeable wall. Here, following Ungarish & Huppert (1998), we must distinguish between two models of particle transport: the turbulent remixing and the laminar settling models (labelled T and L, respectively, in that paper). The latter model bears the greatest similarity to the porous boundary problem because it assumes that the concentration of the particles is constant (i.e. g' does not change during propagation) and the settling of the particle causes 'pure' fluid from the current to flow through the upper interface and mix with the embedding fluid, thus causing a continuous decay of the volume of the current, $\mathscr{V}(t)$. The parameter $\bar{\beta} = h_0/(w_s T)$, where w_s is the particle settling velocity, is analogous to the present λ. However, quantitatively this similarity is not exact: the settling velocity of the particles is constant, while the porous suction velocity is dependent on the local

and instantaneous value of $h(x,t)$. Consequently the particle-driven current is subject to a more effective decay mechanism than the drainage through a porous medium when $\bar{\beta} = \lambda$. The interesting question of how these two effects combine is left for future investigations.

The research was supported by the EPSRC and by the Fund for Promotion of Research at the Technion.

Appendix A. The box model for an impermeable boundary

The limit $\lambda \to 0$ corresponds to the impermeable boundary case. The results are as follows.

A.1. *Rectangular geometry*

In the shallow stage,

$$x_N(t) = (\tfrac{7}{12}\mathscr{H}^{1/3}t + 1)^{6/7} \quad (t \leqslant t_*), \tag{A 1}$$

$$t_* = \frac{12}{7\mathscr{H}^{1/3}}\left[\left(\frac{1}{0.075\mathscr{H}}\right)^{7/6} - 1\right] \tag{A 2}$$

and

$$x_* = 1/(0.075\mathscr{H}). \tag{A 3}$$

When $\mathscr{H} \geqslant 1/0.075$ and the shallow stage does not occur, we define $t_* = 0$ and $x_* = 1$. For the deep stage of propagation

$$x_N(t) = [\tfrac{3}{2}1.19(t - t_*) + x_*^{3/2}]^{2/3} \quad (t \geqslant t_*). \tag{A 4}$$

In both stages $h_N(t) = 1/x_N(t)$.

A.2. *Cylindrical (axisymmetric) geometry*

In the shallow stage,

$$r_N(t) = (\tfrac{2}{3}\mathscr{H}^{1/3}t + 1)^{3/4} \quad (t \leqslant t_*), \tag{A 5}$$

$$t_* = \frac{3}{2\mathscr{H}^{1/3}}\left[\left(\frac{1}{0.075\mathscr{H}}\right)^{2/3} - 1\right] \tag{A 6}$$

and

$$r_* = 1/(0.075\mathscr{H})^{1/2}. \tag{A 7}$$

When $\mathscr{H} \geqslant 1/0.075$ and the shallow stage does not occur, we define $t_* = 0$ and $r_* = 1$. For the deep stage of propagation

$$r_N(t) = [1.19 \times 2(t - t_*) + r_*^2]^{1/2} \quad (t \geqslant t_*). \tag{A 8}$$

In both stages $h_N(t) = 1/r_N^2(t)$.

REFERENCES

Anderson, D. A., Tannehill, J. C. & Pletcher, R. M. 1984 *Computational Fluid Mechanics and Heat Transfer*. Hemisphere.

Benjamin, T. B. 1968 Gravity currents and related phenomena. *J. Fluid Mech.* **31**, 209–248.

Bonnecaze, R. T., Hallworth, M. A., Huppert, H. E. & Lister, J. R. 1995 Axisymmetric particle-driven gravity currents. *J. Fluid Mech.* **294**, 93–121.

Bonnecaze, R. T., Huppert, H. E. & Lister, J. R. 1993 Particle-driven gravity currents. *J. Fluid Mech.* **250**, 339–369.

Davis, S. H. & Hocking, L. M. 1999 Spreading and imbition of viscous liquid on a porous base. *Phys. Fluids* **11**, 48–57.

Hogg, A., Ungarish, M. & Huppert, H. E. 2000 Particle-driven gravity currents: asymptotic and box model solutions. *Eur. J. Mech.* B/*Fluids* **19**, 139–165.

Huppert, H. E. 1982 The propagation of two-dimensional and axisymmetric viscous gravity currents over a rigid horizontal surface. *J. Fluid Mech.* **121**, 43–58.

Huppert, H. E. 1998 Quantitative modelling of granular suspension flows. *Phil. Trans. R. Soc. Lond.* A **356**, 2471–2496.

Huppert, H. E. & Simpson, J. E. 1980 The slumping of gravity currents. *J. Fluid Mech.* **99**, 785–799.

Simpson, J. E. 1997 *Gravity Currents in the Environment and the Laboratory*. Cambridge University Press.

Sparks, R. S. J., Bonnecaze, R. T., Huppert, H. E., Lister, J. R., Hallworth, M. A., Mader, H. & Phillips, J. C. 1993 Sediment-laden gravity currents with reversing buoyancy. *Earth. Planet. Sci. Lett.* **114**, 243–257.

Thomas, L. P., Marino, B. M. & Linden, P. F. 1998 Gravity currents over porous substrate. *J. Fluid Mech.* **366**, 239–258.

Ungarish, M. & Huppert, H. E. 1998 The effect of rotation on axisymmetric gravity currents. *J. Fluid Mech.* **362**, 17–51.